Available online at www.sciencedirect.com
ScienceDirect
Journal of Computational Physics 227 (2008) 2463–2480
JOURNAL OF COMPUTATIONAL PHYSICS
www.elsevier.com/locate/jcp

ADER schemes for the shallow water equations in channel with irregular bottom elevation

G. Vignoli [a,*], V.A. Titarev [b], E.F. Toro [c]

[a] CISMA srl. c/o TIS Innovation Park, via Siemens 19, Bolzano, Italy
[b] Fluid Mechanics and Computational Science Group (FMaCS), Department of Aerospace Sciences, School of Engineering, Cranfield University, UK
[c] Laboratory of Applied Mathematics, Faculty of Engineering, University of Trento, Trento, Italy

Received 29 December 2006; received in revised form 3 August 2007; accepted 1 November 2007
Available online 17 November 2007

Abstract

This paper deals with the construction of high-order ADER numerical schemes for solving the one-dimensional shallow water equations with variable bed elevation. The non-linear version of the schemes is based on ENO reconstructions. The governing equations are expressed in terms of total water height, instead of total water depth, and discharge. The ENO polynomial interpolation procedure is also applied to represent the variable bottom elevation. ADER schemes of up to fifth order of accuracy in space and time for the advection and source terms are implemented and systematically assessed, with particular attention to their convergence rates. Non-oscillatory results are obtained for discontinuous solutions both for the steady and unsteady cases. The resulting schemes can be applied to solve realistic problems characterized by non-uniform bottom geometries.

Keywords: Shallow water; Bottom variation; Source terms; High-order methods; ENO; Godunov's method; Derivative Riemann problem; ADER

1. Introduction

There is a wide range of physical situations, such as flows in open channels and rivers, that can be mathematically represented by first-order non-linear systems of partial differential equations, whose derivation involves an assumption of the *shallow water type*. With rare exceptions, the governing equations are hyperbolic. The loss of hyperbolicity may occur in models of the multi-layer type, for which the equations are of mixed elliptic–hyperbolic type. Hyperbolicity and non-linearity mean that even for smooth initial conditions the solution may exhibit shock waves, or bores. Godunov-type methods, first developed in the aerospace industry to solve the compressible Euler equations, have steadily been exported to other application areas,

* Corresponding author.
E-mail address: gianluca.vignoli@cisma.bz.it (G. Vignoli).

0021-9991/$ - see front matter © 2007 Elsevier Inc. All rights reserved.
doi:10.1016/j.jcp.2007.11.006

including shallow water type flows. Early works in this direction are, for example, [25,26,10,1,11,8,9]. An informative paper is [34], in which a large number of numerical methods for the one-dimensional shallow water equations are implemented and assessed. Further information on Godunov schemes for the shallow water equations is found in the textbook [27] and references therein.

Realistic shallow water type models will include source terms, that is, non-differential terms that are functions of the vector of unknowns. For sometime it has been accepted that the discretization of source terms can be as challenging as for the non-linear advection terms. It must be said that for most cases, even naive discretizations for source terms work reasonably well, but there are some well documented situations in which only sophisticated schemes can perform adequately. When solving real problems one is likely to encounter all sorts of situations, with a high probability that naive schemes will compromise the quality and reliability of the solution.

Difficulties in discretizing source terms are present at the first-order level. A separate issue is that of constructing schemes of higher order of accuracy. In view of Godunov's theorem [12], this is difficult even for equations without source terms, and schemes of second or higher order must necessarily be non-linear to avoid the production of unphysical oscillations in the vicinity of large spatial gradients. There are currently good second-order schemes for the shallow water equations, although it is sometimes difficult to ascertain whether the second order of accuracy is valid for all the terms involved or not.

In this paper, we study numerical methods that address these two difficulties, namely (i) source terms and (ii) high order of accuracy. There have been some works in this direction. For example, ENO and WENO methods have already been applied to the shallow water equations; see for instance [3].

Here we are concerned with ADER type schemes. These methods of arbitrary accuracy were first introduced in [28] for linear problems in one and multiple space dimensions and then further developed for non-linear problems in, for example, [22,29,30,24]. Further developments of ADER schemes are also reported in [21,18,19,17,14–16,6,4].

The ADER methodology is a Godunov-type approach in which the numerical flux uses the solution of the so-called derivative Riemann problem (DRP) [29,31]. In this type of Riemann problems the initial conditions consist of two variable vectors either side of the initial discontinuity, instead of two constant vectors, as in the classical Godunov method. In the solution of the intercell DRP to compute the numerical flux, the influence of the source term is included, that is, the numerical flux knows of the source term. Then the numerical source term is computed from a volume integral evaluated on high-order solutions in space and time, within the space–time volume. In this manner ADER schemes of arbitrary order of accuracy for the coupled non-linear advection and source terms can be constructed. Preliminary results on the ADER method for the shallow water equations are presented in [23,30].

In this paper, we report on ADER schemes based on ENO non-linear reconstructions for the shallow water equations with source terms due to bottom variation. The objective is to construct high-order, well-balanced non-oscillatory schemes. Well-balanced schemes are constructed using (i) a suitable formulation of the governing equations and (ii) a staggered grid. The free surface elevation and water discharge are defined at the centre of the volume, while the bottom elevation is defined at the volume interfaces. The source term and the numerical fluxes are then evaluated using the solution of the derivative Riemann problem [29,31]. The resulting ADER schemes are of arbitrary order of accuracy and are applicable to smooth and discontinuous solutions, both steady and unsteady.

The rest of the paper is as follows. Section 2 is about the governing equations and its reformulation. Section 3 describes the numerical methods of this paper. Numerical results are presented in Section 4. In Section 5, we carry out a systematic convergence rate study of the numerical algorithms proposed. A summary and concluding remarks are found in Section 6. Appendix that illustrates the Cauchy–Kowalewski procedure for the equations of interest here.

2. Formulation of the problem

The shallow water equations can be written in conservative form for the simple case of an horizontal bed channel and vanishing bottom friction in terms of the water depth D and water discharge Q in the following form [32,10]:

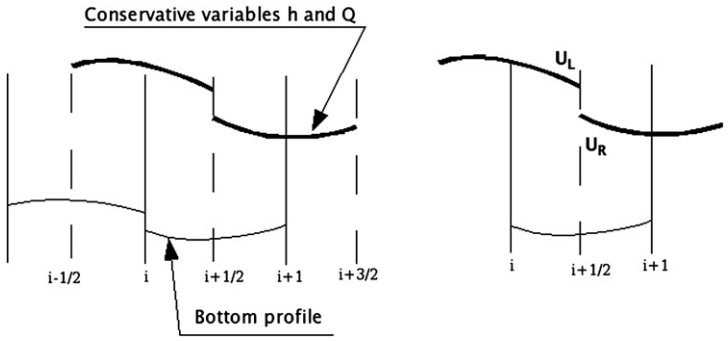

Fig. 1. Formulation of the problem, data reconstruction (left), control volume and derivative Riemann problem (right).

$$\begin{cases} \frac{\partial D}{\partial t} + \frac{\partial Q}{\partial x} = 0, \\ \frac{\partial Q}{\partial t} + \frac{\partial}{\partial x}\left(\frac{Q^2}{D} + \frac{1}{2} g D^2\right) = -gD\frac{\partial b}{\partial x}, \end{cases} \tag{1}$$

where $b(x)$ is the bottom elevation, t and x are the temporal and spatial independent variables, respectively, and g is the acceleration due to gravity. See Fig. 1, where a longitudinal profile representing a couple of computational cells is depicted.

It is known that when the equations include source terms standard numerical schemes applied to (1) do not perform satisfactorily, particularly for the steady-state case. This is because only the relative position between the free surface and the bed profile is known and the information regarding the absolute position of the free surface (or of the bed) is lost. There are two physical situations of interest here; one in which the particle velocity is zero, which we call stationary flow, and one in which temporal partial derivatives in (1) are identically zero, steady flow. We note that standard explicit schemes for the shallow water with source terms, if convergent, converge very slowly to the correct steady-state solution, and consequently, very fine meshes are required for obtaining satisfactory results.

To design a numerical method capable of reproducing both steady and unsteady solutions we follow the formulation of the equations reported in [33], using the free surface elevation $H = D + b$ as an unknown, with which (1) becomes

$$\begin{cases} \frac{\partial H}{\partial t} + \frac{\partial Q}{\partial x} = 0, \\ \frac{\partial Q}{\partial t} + \frac{\partial}{\partial x}\left(\frac{Q^2}{H-b} + \frac{1}{2} g H^2 - gbH\right) = -gH\frac{\partial b}{\partial x}. \end{cases} \tag{2}$$

System (2) is hyperbolic with eigenvalues $\lambda^{(i)}$ and right eigenvectors $R^{(i)}$:

$$\lambda^{(1)} = u - a, \lambda^{(2)} = u + a, \quad \mathbf{R}^{(1)} = \begin{pmatrix} 1 \\ u - a \end{pmatrix}, \quad \mathbf{R}^{(2)} = \begin{pmatrix} 1 \\ u + a \end{pmatrix},$$

where $u = Q/D$ is the flow velocity and $a = \sqrt{gD}$ is the celerity.

The two main advantages of formulation (2) are that the model reproduces in the correct manner the physics of the problem, and it allows us to use existing Riemann solvers, such as the exact Riemann solver in [27], for the evaluation of the numerical fluxes between neighbouring computational volumes.

3. Numerical scheme

System (2) can be written in the following conservative form:

$$\frac{\partial \mathbf{U}}{\partial t} + \frac{\partial \mathbf{F}}{\partial x} = \mathbf{S}, \tag{3}$$

where the unknown vector $\mathbf{U}$, the flux vector $\mathbf{F}$ and the source term $\mathbf{S}$ are given by

$$\mathbf{U} = \begin{pmatrix} H \\ Q \end{pmatrix}, \quad \mathbf{F} = \begin{pmatrix} Q \\ \frac{Q^2}{H-b} + \frac{1}{2}gH^2 - gHb \end{pmatrix}, \quad \mathbf{S} = \begin{pmatrix} 0 \\ -gH\frac{\partial b}{\partial x} \end{pmatrix}.$$

Integration of (3) over the control volume $I_i = [x_{i-\frac{1}{2}}, x_{i+\frac{1}{2}}] \times [t^n, t^{n+1}]$ on the x–t plane gives

$$\mathbf{U}_i^{n+1} = \mathbf{U}_i^n - \frac{\Delta t}{\Delta x}\left(\mathbf{F}_{i+\frac{1}{2}} - \mathbf{F}_{i-\frac{1}{2}}\right) + \Delta t \mathbf{S}_i. \tag{4}$$

Here $\mathbf{U}_i^n$ is the cell average of the solution at time level t^n, $\mathbf{F}_{i+\frac{1}{2}}$ is the time average of the flux at cell interface $x_{i+\frac{1}{2}}$ and $\mathbf{S}_i$ is the time–space average of the source term over the control volume, namely

$$\begin{aligned} \mathbf{U}_i^n &= \frac{1}{\Delta x}\int_{x_{i-\frac{1}{2}}}^{x_{i+\frac{1}{2}}} \mathbf{U}(x, t^n)\mathrm{d}x, \quad \mathbf{F}_{i+\frac{1}{2}} = \frac{1}{\Delta t}\int_{t^n}^{t^n+\Delta t} \mathbf{F}\left(x_{i+\frac{1}{2}}, t\right)\mathrm{d}t, \\ \mathbf{S}_i &= \frac{1}{\Delta t \Delta x}\int_{t^n}^{t^n+\Delta t}\int_{x_{i-\frac{1}{2}}}^{x_{i+\frac{1}{2}}} \mathbf{S}(x,t)\mathrm{d}x\,\mathrm{d}t. \end{aligned} \tag{5}$$

To construct a numerical method for the solution of (3) we need to define suitable approximations to $\mathbf{F}_{i+\frac{1}{2}}$ and to $\mathbf{S}_i$, preserving the same notation, which are then called the *numerical flux* and the *numerical source*, respectively. We use the cell centred approach for the unknown vector $\mathbf{U}$, while for the bottom elevation, which appears in the formulation for the fluxes $\mathbf{F}_{i+\frac{1}{2}}$ and for the source terms $\mathbf{S}_i$, we use an interface-centred approach; the averaged values $b_{i+\frac{1}{2}}$ are defined as

$$b_{i+\frac{1}{2}} = \frac{1}{\Delta x}\int_{x_i}^{x_{i+1}} b(x)\mathrm{d}x. \tag{6}$$

To develop high-order numerical schemes we use the ADER approach for the evaluation of the numerical fluxes and of the numerical source. The ADER approach consists of three steps: (i) reconstruction of high-degree polynomials starting from the cell average values of the solution; (ii) solution of the derivative Riemann problem and evaluation of the intercell flux $\mathbf{F}_{i+\frac{1}{2}}$; (iii) evaluation of the numerical source $\mathbf{S}_i$ by a high-order computation of the space–time integral inside the control volume.

Pointwise values of the solution at time level t^n are found from the reconstructed high-degree polynomials. In this paper we use the ENO [13,20] reconstruction procedure to avoid spurious oscillations, leading to a non-linear numerical scheme. We note that the reconstruction is performed both for the unknown vector $\mathbf{U}$ and for the bottom elevation b (only once), as depicted in Fig. 1.

After the data reconstruction procedure we solve the following derivative Riemann problem (DRP):

$$\begin{aligned} &\partial_t \mathbf{U} + \partial_x \mathbf{F}(\mathbf{U}) = \mathbf{S}(\mathbf{U}), \\ &\mathbf{U}(x,0) = \begin{cases} \mathbf{p}_i(x), & x < x_{i+\frac{1}{2}}, \\ \mathbf{p}_{i+1}(x), & x > x_{i+\frac{1}{2}} \end{cases} \end{aligned} \tag{7}$$

to find the solution at $x = x_{i+\frac{1}{2}}$, denoted by $\mathbf{U}_{i+\frac{1}{2}}(\tau)$, where $\mathbf{p}_i(x)$ denotes the vector of reconstructed polynomials in ith cell. Note that the value $b_{i+\frac{1}{2}}$ as well as its spatial derivatives are known. Following [29,31] we find the approximate flux at cell interface using an appropriate Gaussian rule:

$$\mathbf{F}_{i+\frac{1}{2}} = \sum_{\alpha=0}^{N} \mathbf{F}\left(\mathbf{U}_{i+\frac{1}{2}}(\gamma_\alpha \Delta t)\right) K_\alpha, \tag{8}$$

where γ_α are suitable Gaussian coefficients, and K_α are Gaussian weights. The solution $\mathbf{U}_{i+\frac{1}{2}}(\tau)$ of the DRP problem (7) is found by first expressing it as a Taylor series expansion:

$$\begin{aligned} \mathbf{U}_{i+\frac{1}{2}}(\tau) &= \mathbf{U}\left(x_{i+\frac{1}{2}}, 0^+\right) + \sum_{k=1}^{r}\left[\partial_t^{(k)}\mathbf{U}\left(x_{i+\frac{1}{2}}, 0^+\right)\frac{\tau^k}{k!}\right], \\ \partial_t^{(k)}\mathbf{U}\left(x_{i+\frac{1}{2}}, 0^+\right) &= \frac{\partial^k}{\partial t^k}\mathbf{U}\left(x_{i+\frac{1}{2}}, 0^+\right), \end{aligned} \tag{9}$$

where $0^+ = \lim_{t\to 0^+} t$. The leading term $\mathbf{U}(x_{i+\frac{1}{2}}, 0^+)$ is found by solving the classical homogeneous Riemann problem with piecewise constant data:

$$\partial_t \mathbf{U} + \partial_x \mathbf{F}(\mathbf{U}) = \mathbf{0}, \quad \mathbf{U}(x,0) = \begin{cases} \mathbf{p}_i\left(x_{i+\frac{1}{2}}\right), & x < x_{i+\frac{1}{2}}, \\ \mathbf{p}_{i+1}\left(x_{i+\frac{1}{2}}\right), & x > x_{i+\frac{1}{2}} \end{cases} \tag{10}$$

and evaluating its solution at $(x - x_{i+\frac{1}{2}})/t = 0$ to obtain $\mathbf{U}(x_{i+\frac{1}{2}}, 0^+)$, the so-called Godunov state, which in this paper is evaluated using the exact Riemann solver [27]. The remaining terms in (9) are computed by replacing all time derivatives $\partial_t^{(k)}\mathbf{U}(x_{i+\frac{1}{2}}, 0^+)$ by functions of spatial derivatives $\partial_x^{(l)}\mathbf{U}(x_{i+\frac{1}{2}}, 0^+)$ using the Cauchy–Kowalewski procedure, reported in Eqs. (21)–(23). Now the problem of computing time derivatives is replaced by that of determining spatial derivatives of the conservative variables H and Q.

The unknown spatial derivatives at $t = 0^+$ are found from the following linearized Riemann problems:

$$\begin{aligned} &\partial_t\left(\partial_x^{(k)}\mathbf{U}\right) + \mathbf{A}\left(\mathbf{U}\left(x_{i+\frac{1}{2}}, 0^+\right)\right)\partial_x\left(\partial_x^{(k)}\mathbf{U}\right) = \mathbf{0}, \quad \mathbf{A}(\mathbf{U}) = \frac{\partial \mathbf{F}}{\partial \mathbf{U}}, \\ &\partial_x^{(k)}\mathbf{U}(x,0) = \begin{cases} d^{(k)}\mathbf{p}_i\left(x_{i+\frac{1}{2}}\right), & x < x_{i+\frac{1}{2}}, \\ d^{(k)}\mathbf{p}_{i+1}\left(x_{i+\frac{1}{2}}\right), & x > x_{i+\frac{1}{2}}, \end{cases} \end{aligned} \tag{11}$$

where $\mathbf{A}(\mathbf{U})$ is the Jacobian of the system and is given in the Appendix and the symbol $d^{(k)}$ denotes the kth derivative with respect to the spatial variable x. The boundary extrapolated values are found using the polynomials $\mathbf{p}_i(x)$, $\mathbf{p}_{i+1}(x)$ obtained by the ENO reconstruction procedure.

The first component of the source term (i.e. the source for the continuity equation) is equal to zero. To evaluate the second component of the source term we first perform integration by parts:

$$\begin{aligned} \mathbf{S}_i^{(2)} &= \frac{1}{\Delta t \Delta x}\int_0^{\Delta t}\int_{x_{i-\frac{1}{2}}}^{x_{i+\frac{1}{2}}}\left(-gH\frac{\partial b}{\partial x}\right)\mathrm{d}x\,\mathrm{d}t \\ &= -\frac{g}{\Delta t}\int_0^{\Delta t}\left(Hb|_{x_{i+\frac{1}{2}}} - Hb|_{x_{i-\frac{1}{2}}}\right)\mathrm{d}t + \frac{g}{\Delta t \Delta x}\int_0^{\Delta t}\int_{x_{i-\frac{1}{2}}}^{x_{i+\frac{1}{2}}} b\frac{\partial H}{\partial x}\mathrm{d}x\,\mathrm{d}t \end{aligned} \tag{12}$$

The first part is evaluated using suitable Gaussian points and a Taylor time expansion for the evaluation of $H(x_{i\pm\frac{1}{2}}, t)$. The second integral in (12) is approximated by a Gaussian integration rule:

$$\frac{g}{\Delta x \Delta t}\int_0^{\Delta t}\int_{x_{i-\frac{1}{2}}}^{x_{i+\frac{1}{2}}} b\frac{\partial H}{\partial x}\mathrm{d}x\,\mathrm{d}t = g\sum_{\alpha=1}^{N}\left[\sum_{l=1}^{N}\left(b(x_\alpha)\frac{\partial}{\partial x}H(x_\alpha, \tau_l)\right)K_l\right]K_\alpha. \tag{13}$$

We note that the evaluation of (13) is not necessary for the first-order version of the scheme. Integral (13) must be evaluated by splitting the space integral in two parts: $x_{i-\frac{1}{2}} - x_i$ and $x_i - x_{i+\frac{1}{2}}$, because the representation of the bed elevation $b(x)$ is given by an interface-centred approach and consequently, two different reconstructed polynomials for $b(x)$ are present in cell i.

3.1. Conservative property and source terms

It is obvious that the governing equations contain non-vanishing terms also in the case of steady flow. Under stationary conditions in the momentum equation, both the source term due to the bottom elevation $-gH\frac{\partial b}{\partial x}$ and the flux term due to hydrostatic pressure $\frac{1}{2}gH^2 - gHb$ are different from zero and the former balances the divergence of the latter.

A numerical method capable of reproducing the exact solution under steady conditions is said to satisfy the $\mathcal{C}$-property; the method is said to satisfy the approximate $\mathcal{C}$-property if it is accurate up to the prescribed order when applied to a steady problem [32]. The stationary solution, characterized by vanishing velocities everywhere in the domain, is a subset of the steady solutions. If the numerical scheme reproduces the exact solution in this case (water free surface at rest, i.e. $H = \text{constant}$, $Q = u = 0$) it is said

to satisfy the $\mathcal{Z}$-property. The scheme proposed in this paper satisfies the $\mathcal{Z}$-property and the approximate $\mathcal{C}$-property.

We note that when $H = H_0 = \text{constant}$, $Q = 0$ and $u = 0$ in the whole domain, the reconstructed values $\mathbf{p}_i(x)$ and $\mathbf{p}_{i+1}(x)$ are equal to $H = H_0$, $Q = 0$ at all the interfaces between numerical cells. Moreover, reconstructed values for all the spatial derivatives of H and Q are equal to zero. We can now compute the numerical fluxes, following the situation depicted in Fig. 1:

$$\mathbf{F}_{i-\frac{1}{2}} = \begin{pmatrix} 0 \\ \frac{1}{2} g H^2_{i-\frac{1}{2}} + g H_{i-\frac{1}{2}} b_{i-\frac{1}{2}} \end{pmatrix}, \quad \mathbf{F}_{i+\frac{1}{2}} = \begin{pmatrix} 0 \\ \frac{1}{2} g H^2_{i+\frac{1}{2}} + g H_{i+\frac{1}{2}} b_{i+\frac{1}{2}} \end{pmatrix}.$$

The source term is then evaluated using integration by parts, and recalling that the spatial derivative of the reconstructed variable H is zero:

$$\mathbf{S}_i^{(2)} = -\frac{g}{\Delta x \Delta t} \int_{t^n}^{t^n+\Delta t} \int_{x_{i-\frac{1}{2}}}^{x_{i+\frac{1}{2}}} H \frac{\partial b}{\partial x} \mathrm{d}x \, \mathrm{d}t = \frac{g}{\Delta t} \int_{t^n}^{t^n+\Delta t} \left(bH|_{x-\frac{1}{2}} - bH|_{x+\frac{1}{2}} \right) \mathrm{d}t = g \left(bH|_{x-\frac{1}{2}} - bH|_{x+\frac{1}{2}} \right). \tag{14}$$

Applying scheme (4) it is easy to show that the numerical scheme reproduces the exact solution. The numerical results shown in Fig. 2 verify the stated property of the scheme.

4. Numerical solutions

The numerical method is tested to verify that both steady and unsteady solutions are well reproduced. The latter case is traditionally associated with dam-break problems, characterized by the propagation of sharp fronts. In the former case both smooth and discontinuous solutions can be observed. Results reported in this paper are computed using Courant number CFL = 0.9, moreover, steady solutions have been obtained by marching in time to steady state, starting from an initial profile (horizontal free surface profile) that is far away from the steady solution.

4.1. Steady solutions

For the test under steady conditions there are several different configurations characterized by smooth or discontinuous solutions, depending on the values of the water discharge Q, the maximum height of the bed

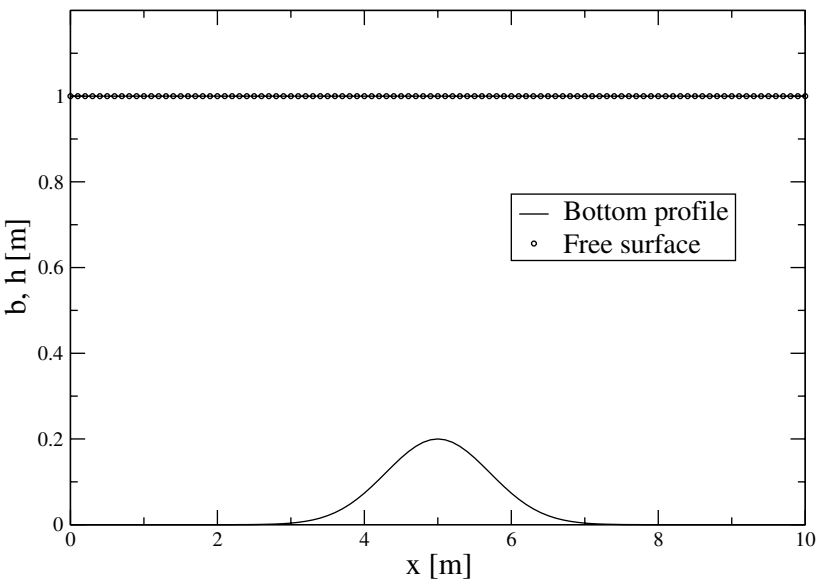

Fig. 2. Computed stationary state solution for the flow over a non horizontal bed with initial condition equal to $H = 1$ m, $Q = 0$ m^2 s^{-1}, $u = 0$ m/s, $L = 10$ m and $b(x) = b_{\max} \cdot \exp[-\frac{(x-L/2)^2}{(L/2)^2}]$, $b_{\max} = 0.2$ m, CFL = 0.9.

profile b_{max} and the boundary conditions for the free surface elevation $H(x = 0)$ and $H(x = L)$, where L is the channel length. Figs. 3 and 4 show the numerical results for free surface elevation and water discharge, respectively, obtained with a fifth-order ADER method, for the standard test case of subcritical flow over a parabolic bump. This solution is computed choosing a maximum bed elevation such that the flow remains subcritical in the domain and the solution does not exhibit discontinuities. This is the case of the flow field in large rivers, where the irregular geometry produces small flow disturbances. The numerical method is able

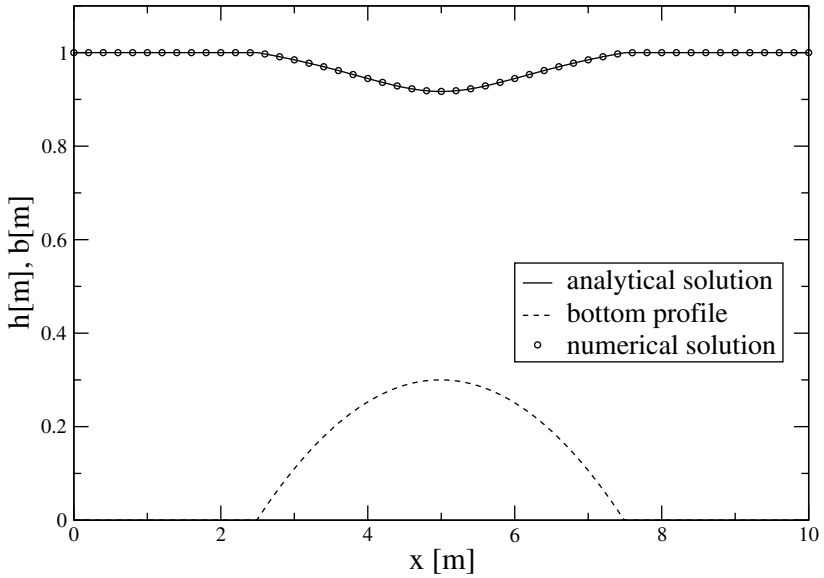

Fig. 3. *Steady case*: free surface elevation in the case of smooth solution and parabolic bed profile $b(x) = \max(0, -16b_{max}/L^2(x^2 - Lx) - 3b_{max})$. ADER (fifth order) numerical method used. ($Q = 1\ m^2\ s^{-1}$, $b_{max} = 0.3$ m, $H(x = L) = 1$ m, $N = 50$, $L = 10$ m, CFL $= 0.9$.)

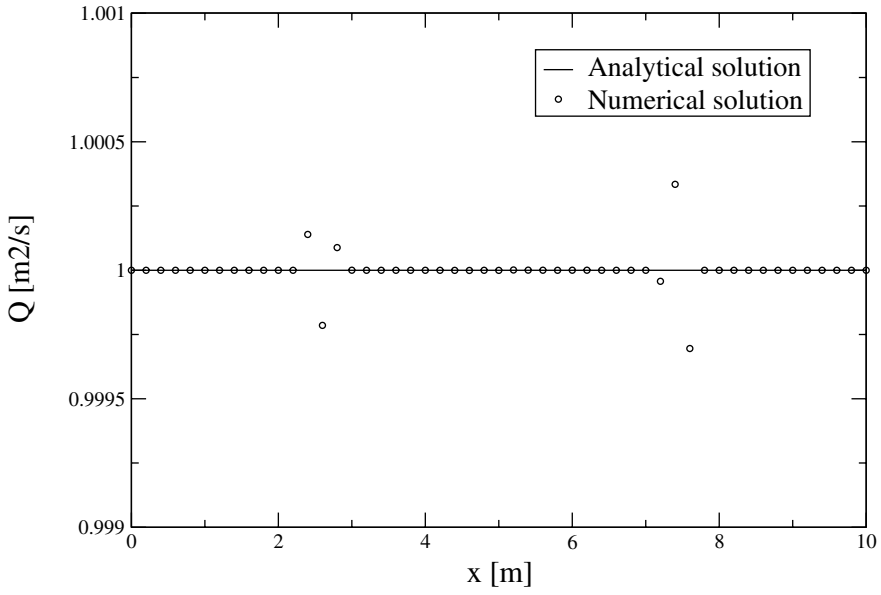

Fig. 4. *Steady case*: water discharge in the case of smooth solution and parabolic bed profile $b(x) = \max(0, -16b_{max}/L^2(x^2 - Lx) - 3b_{max})$. ADER (fifth order) numerical method used. ($Q = 1\ m^2\ s^{-1}$, $b_{max} = 0.3$ m, $H(x = L) = 1$ m, $N = 50$, $L = 10$ m, CFL $= 0.9$.)

to compute very accurately the local flow acceleration and the perturbation of the free surface elevation. However, as seen in Fig. 4, the computed discharge exhibits small but visible errors.

For larger values of the elevation of the bump the free surface profile becomes steeper and steeper until it becomes discontinuous. This is the case shown in Figs. 5 and 6, where the maximum bottom elevation is 0.5 m. The numerical solution of Figs. 5 and 6 agrees with the exact solution both for the free surface elevation and the water discharge.

We remark that for the case of steady and discontinuous solutions, the position of the shock is stationary and depends on the water discharge, the maximum bottom elevation and the boundary conditions. It is possible to obtain a more accurate numerical solution (as plotted in the upper part of Fig. 5) if the mesh is chosen

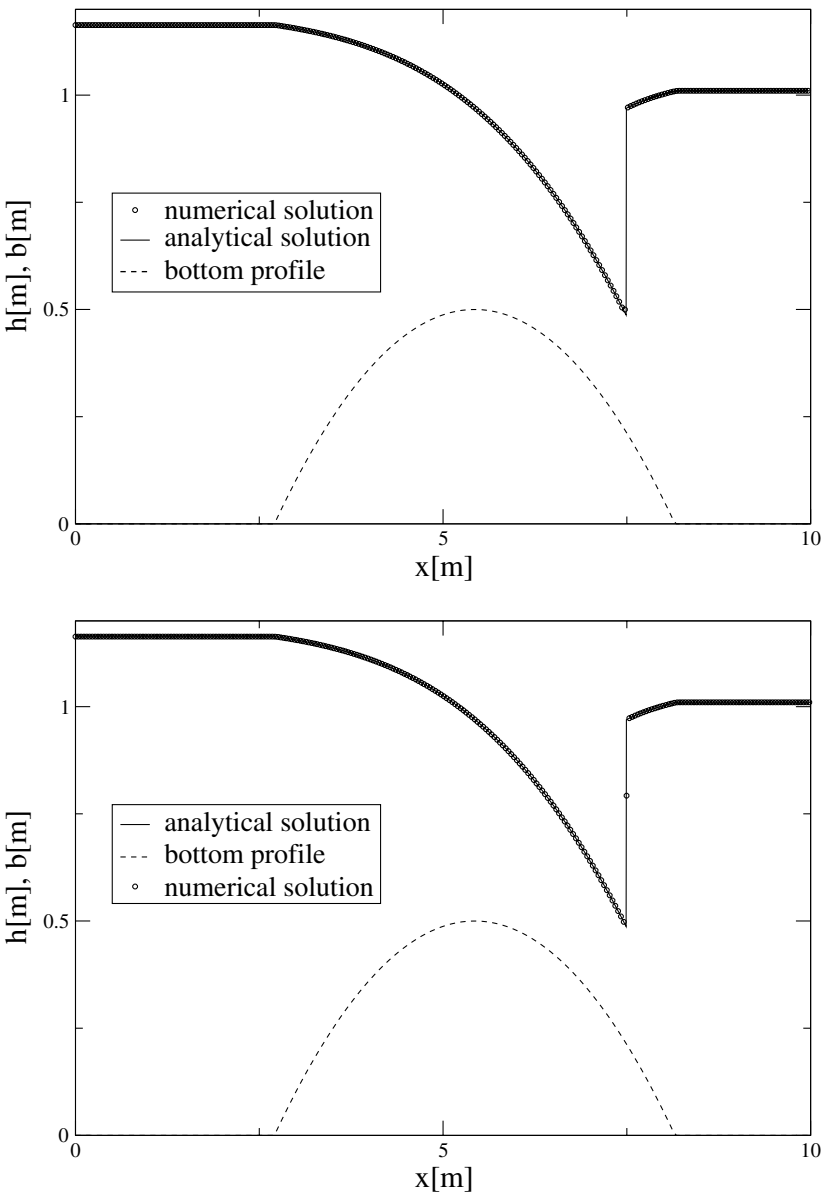

Fig. 5. *Steady case*: free surface elevation in the case of discontinuous solution and parabolic bed profile $b(x) = \max(0, -16b_{\max}/L^2(x^2 - Lx) - 3b_{\max})$. ADER (fifth order) numerical method used. ($Q = 1\ \mathrm{m^2\ s^{-1}}$, $b_{\max} = 0.5$ m, $H(x = L) = 1$ m, top $N = 280$, bottom $N = 285$, $L = 10$ m, CFL $= 0.9$.)

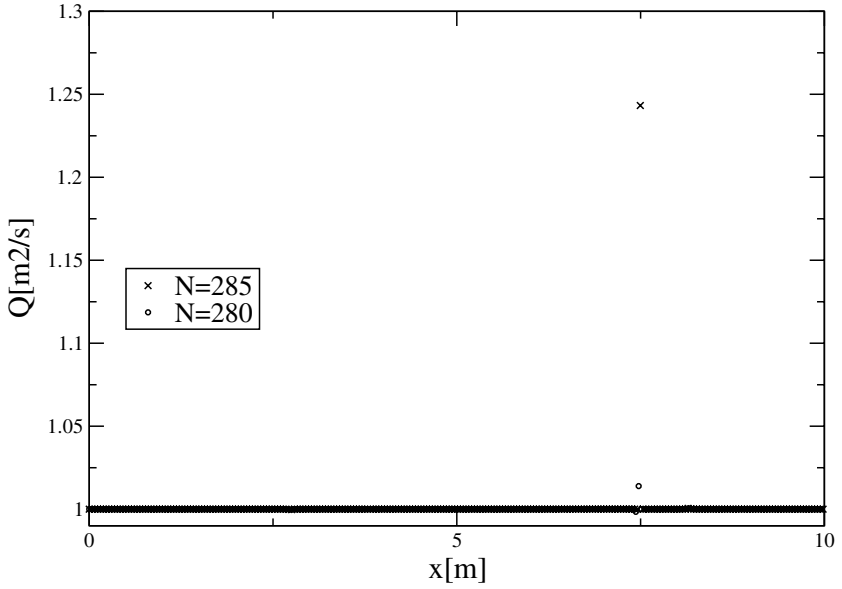

Fig. 6. *Steady case*: water discharge in the case of discontinuous solution and parabolic bed profile $b(x) = \max(0, -16b_{\max}/L^2(x^2 - Lx) - 3b_{\max})$ with two meshes $N = 280$ and $N = 285$. ADER (fifth order) numerical method used. ($Q = 1\ \mathrm{m^2\ s^{-1}}$, $b_{\max} = 0.5$ m, $H(x = L) = 1$ m, $L = 10$ m, CFL = 0.9.)

in such a way that the shock is positioned precisely at the interface between two adjacent cells, in this case $N = 280$. Note that this procedure is not general because the position of the shock is not known a priori. In other words, for the steady shock solution refinement of the mesh does not always give more accurate results for the shock, as can be seen from Figs. 5 and 6.

4.2. Unsteady solutions

Unsteady solutions are the typical case for which in the past shock capturing numerical method have been constructed. In natural rivers and channels unsteady solutions with a low degree of temporal variability, like flood waves, are due to rainfall events. Rapid phenomena characterized by the formation of sharp fronts and bores are typically related to the presence of artificial structures. Finally, sharp fronts and bores may occur in natural convergent estuaries during the propagation of tidal waves.

4.2.1. Comparison with the exact unsteady Riemann problem solution

Test cases under unsteady conditions are typically dam-break problems. For this kind of problems the analytical solution is available both for the case of horizontal bed profile and for the case of a step-like bottom. The first case has not been considered because for such case our formulation reduces to the standard shallow water formulation. Instead we consider a dam-break test problem over a step-like bottom profile for which the exact solution is available [2]. The test considered has solution characterized by a right-facing shock, a stationary shock and a left-running rarefaction. Fig. 7 shows a comparison between the numerical solution obtained using an ADER (third order) scheme and the exact solution.

Note that in the staggered grid setup of Fig. 1, in the initial condition for the numerical solution the discontinuity for the free surface elevation and for the bottom profile are staggered by half a computational cell. To perform the comparison between numerical and analytical solutions we have used 500 computational cells, such that the space interval between the two discontinuities in the initial condition is sufficiently small. Good agreement is observed, results are essentially non-oscillatory for both shocks. The stationary shock in $x = 0$ m is reproduced with a small error for the water discharge. As for the stationary test case, this error is due to the position of the numerical cell interface.

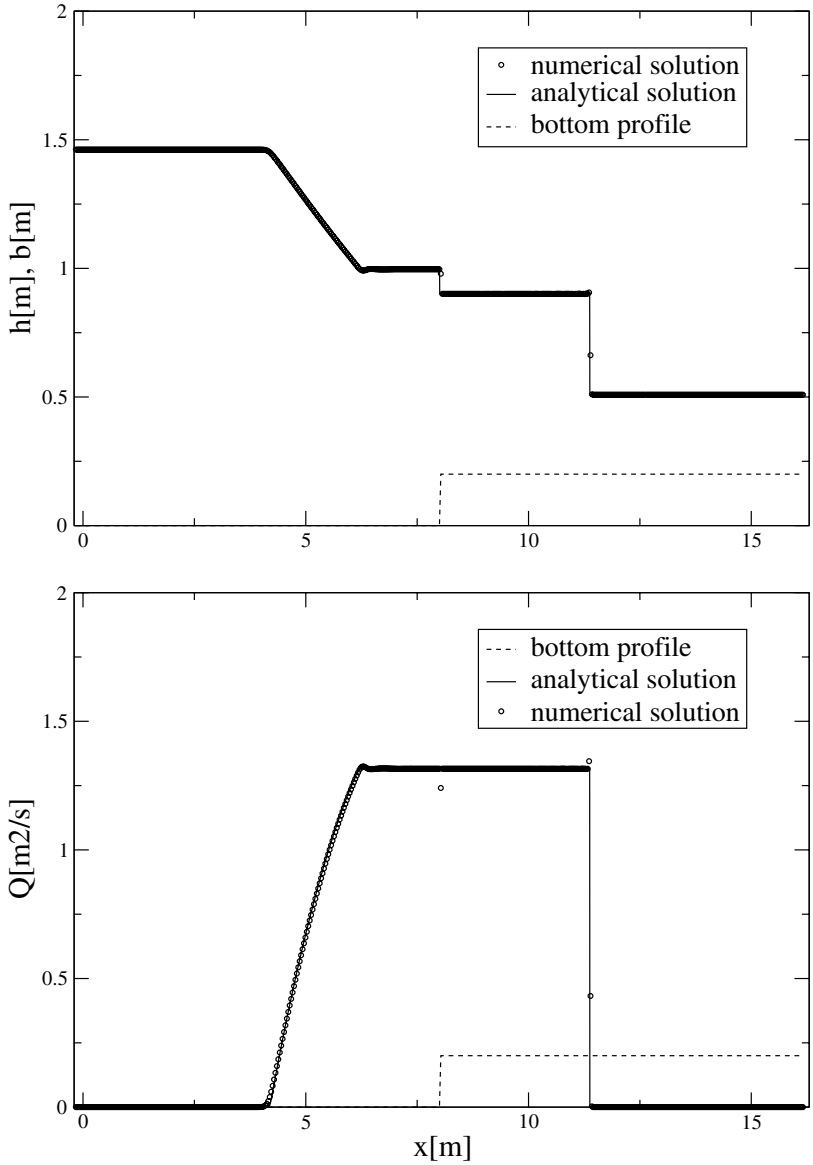

Fig. 7. Comparison between numerical and analytical solutions for the dam-break problem with a bottom step after $T_0 = 1.057$ s. ADER (third order) numerical method used. The initial conditions are $H_L = 1.461837$ m, $H_R = 0.508732$ m and $Q_L = Q_R = 0$ m^2 s^{-1}, the step in the bottom profile is 0.2 m high and is positioned at $x = 8$ m, CFL = 0.9.

4.2.2. Dam-break problem over a smooth bed

As a final example we show numerical results for a dam-break problem over a smooth bed profile. For this case the analytical solution is not available.

Results are shown in Figs. 8 and 9 for the case of a Gaussian bed profile. Under these conditions the solution shows two shock waves. The right-facing shock is due to the initial conditions, while the left-facing shock in the middle of the domain is due to the bottom slope and is *quasi*-stationary.

5. Convergence rates study

In the previous section we have applied our high-order numerical methods to some challenging problems, including shocks, and have shown that the proposed high-order numerical algorithms reproduce well both

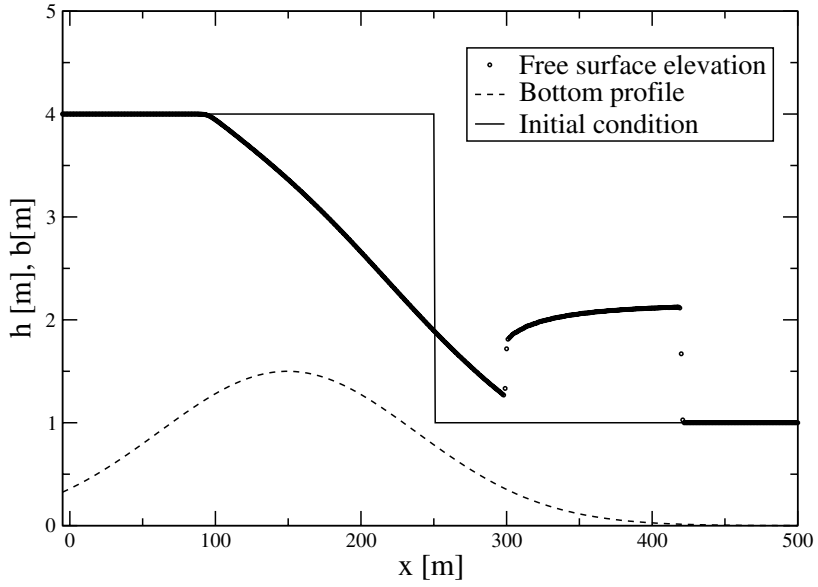

Fig. 8. Solution for dam break over a non horizontal profile $b(x) = b_{\max} \exp[-(\frac{x-150}{128})^2]$, $b_{\max} = 1.5$ m. The initial conditions are $H_L = 4$ m, $H_R = 1$ m and $Q_L = Q_R = 0\ m^2\ s^{-1}$. ADER (third order) numerical method used. The solution at time $T_0 = 40$ s exhibits two shocks. $N = 500$ cells used, CFL = 0.9.

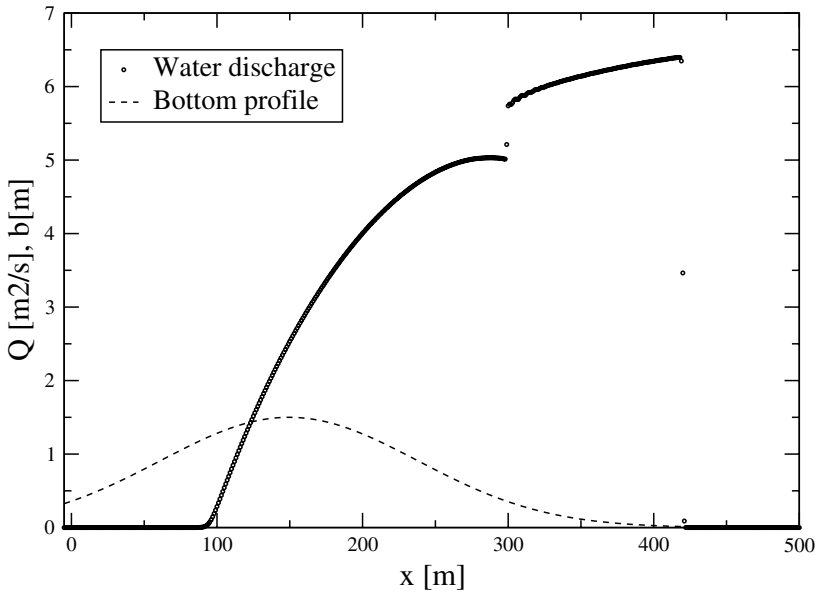

Fig. 9. Solution for dam break over a non horizontal profile $b(x) = b_{\max} \exp[-(\frac{x-150}{128})^2]$, $b_{\max} = 1.5$ m. The initial conditions are $H_L = 4$ m, $H_R = 1$ m and $Q_L = Q_R = 0\ m^2\ s^{-1}$. ADER (third order) numerical method used. The solution at time $T_0 = 40$ s exhibits two shocks. $N = 500$ cells used, CFL = 0.9.

steady and unsteady solutions and the results are essentially non-oscillatory. In this section, we carry out a systematic empirical study of the convergence rates of the schemes to verify that, for smooth solutions, the algorithms are of the claimed theoretical order of accuracy. We do this for both the steady case and unsteady case represented by a full non-linear system with source terms.

We have performed tests for schemes of expected order of accuracy in space and time from second to fifth; for all tests we have used a Courant number coefficient CFL = 0.9, a computational domain of length

$L = 10$ m, with two different bottom topographies, namely bed profiles $b(x)$ described by a Gaussian function and a sinusoidal function. At the outset one can say that results with the sinusoidal bed profile are expected to be better than those obtained using a Gaussian bed profile. As pointed out by Shu [20], in studying convergence rates, difficulties in achieving the expected convergence rates are observed when the involved functions contain large derivatives.

For the tests with a sinusoidal bed profile the computed free surface elevation $H(x,t)$ is a sinusoidal function only if the amplitude of the bottom elevation is small enough. For higher values of the maximum bottom elevation non-linearities in the governing equations give rise to the evolution of more complex free surface profiles exhibiting steeper gradients of the solution $H(x,t)$. For even larger values of the bottom elevation we obtain the limiting case of discontinuous free surface profiles. We also note that for a sinusoidal free surface elevation the second component of the flux is not sinusoidal. All of these considerations suggest that we should test the accuracy of the scheme, both for the steady and the unsteady cases, using small values for the sinusoidal amplitude of the bottom profile.

5.1. Steady case

The numerical scheme is first tested under steady conditions, to verify that it satisfies the approximate $\mathcal{C}$-property.

The empirical rate of convergence of the schemes is tested for a Gaussian and for a sinusoidal bed profile. For the sinusoidal bed profile results are in agreement with the designed order of accuracy of the numerical scheme (see Tables 1 and 2) where we show the result obtained using two different amplitudes for the bed sinusoidal profile, namely 0.001 m and 0.01 m. The expected orders of accuracy are reproduced reasonably for schemes of up to fourth order of accuracy. The fifth-order scheme does not perform as expected, particularly for the largest chosen value of the bottom elevation. As expected, for the Gaussian bed profile the attained order of accuracy does not match the designed one, particularly for the fourth and fifth-order ADER schemes (see Table 3). We note however, that, as expected, the fifth-order scheme is the most accurate in that its errors are the smallest.

Table 1
Convergence rates study for the steady and smooth case, sinusoidal bed profile $b(x) = -b_{\max}\sin(2\pi/Lx)$ and $b_{\max} = 0.001$ m, $Q = 1$ m^2 s^{-1}, $H(x = L) = 1$ m, $L = 10$ m, CFL $= 0.9$

Method	N	$L_{1\,\text{error}}$	$L_{1\,\text{order}}$	$L_{\infty\,\text{error}}$	$L_{\infty\,\text{order}}$
ADER 2	5	0.119E−03		0.252E−03	
	10	0.279E−04	2.09	0.610E−04	2.04
	20	0.616E−05	2.18	0.131E−04	2.21
	40	0.146E−06	2.07	0.297E−05	2.14
	80	0.357E−06	2.03	0.697E−06	2.09
ADER 3	5	0.501E−04		0.111E−03	
	10	0.783E−05	2.67	0.150E−04	2.89
	20	0.998E−06	2.97	0.201E−05	2.89
	40	0.128E−06	2.96	0.257E−06	2.97
	80	0.161E−07	2.98	0.323E−07	2.99
ADER 4	5	0.313E−04		0.703E−04	
	10	0.193E−05	4.02	0.451E−05	3.96
	20	0.114E−05	4.08	0.261E−06	4.10
	40	0.672E−08	4.08	0.150E−07	4.11
	80	0.414E−09	4.02	0.101E−08	3.88
ADER 5	5	0.138E−04		0.322E−04	
	10	0.603E−06	4.51	0.118E−05	4.76
	20	0.206E−07	4.87	0.408E−07	4.86
	40	0.903E−09	4.51	0.142E−08	4.84
	80	0.101E−09	3.15	0.185E−09	2.93

Table 2
Convergence rates study for the steady and smooth case, sinusoidal bed profile $b(x) = -b_{\max}\sin(2\pi/Lx)$ and $b_{\max} = 0.01$ m, $Q = 1\ \mathrm{m^2\ s^{-1}}$, $H(x = L) = 1$ m, $L = 10$ m, CFL = 0.9

Method	N	$L_{1\,\mathrm{error}}$	$L_{1\,\mathrm{order}}$	$L_{\infty\,\mathrm{error}}$	$L_{\infty\,\mathrm{order}}$
ADER 2	5	0.117E−02		0.248E−02	
	10	0.280E−03	2.06	0.606E−03	2.03
	20	0.617E−04	2.18	0.136E−03	2.15
	40	0.146E−04	2.07	0.309E−04	2.13
	80	0.358E−05	2.03	0.729E−05	2.08
ADER 3	5	0.489E−03		0.111E−02	
	10	0.769E−04	2.66	0.148E−03	2.90
	20	0.991E−05	2.95	0.200E−04	2.89
	40	0.128E−05	2.94	0.256E−05	2.96
	80	0.164E−06	2.96	0.323E−06	2.98
ADER 4	5	0.302E−03		0.685E−03	
	10	0.191E−04	3.98	0.440E−04	3.95
	20	0.119E−05	4.00	0.292E−05	3.91
	40	0.720E−07	4.05	0.223E−06	3.71
	80	0.916E−08	2.97	0.262E−07	3.08
ADER 5	5	0.131E−03		0.307E−03	
	10	0.602E−05	4.44	0.114E−04	4.74
	20	0.300E−06	4.32	0.510E−06	4.48
	40	0.386E−07	2.95	0.725E−07	2.81
	80	0.853E−08	2.18	0.169E−07	2.09

5.2. Unsteady case

For the purpose of assessing the convergence rates of the proposed schemes we devise exact, smooth solutions to non-linear inhomogeneous systems in the following manner. We prescribe distributions in space and time for the functions $H(t,x)$ and $Q(t,x)$. These will be exact solutions of a *modified* inhomogeneous system, as we shall see. Inserting these prescribed functions into system (2) produces a *modified system* with an additional source term $\widetilde{S}(x,t)$ due to the fact that $H(x,t)$ and $Q(x,t)$ are not solutions to the original physical system (2) but are exact solutions of the mathematical inhomogeneous system (15). The convergence rates study is performed on the modified system.

The prescribed exact solution is

$$H = H_0 + a_0 \sin\left(2\pi\frac{x}{L}\right)\cos\left(2\pi\frac{t}{T_0}\right),$$
$$Q = Q_0 - \frac{a_0 L}{T_0}\cos\left(2\pi\frac{x}{L}\right)\sin\left(2\pi\frac{t}{T_0}\right)$$

with the bottom elevation given by

$$b = b_0 \sin\left(2\pi\frac{x}{L}\right),$$

where L is the length of the computational domain and T_0 a suitable time period. The resulting artificial source term is computed numerically in the same way as the physical source term. We remark that to use this approach for studying convergence rates one necessarily requires schemes that are able to solve systems with source terms to the expected accuracy, even if the original purpose was to solve homogeneous problems to high accuracy.

The *modified* equations reads

$$\begin{cases} \frac{\partial H}{\partial t} + \frac{\partial Q}{\partial x} = 0, \\ \frac{\partial Q}{\partial t} + \frac{\partial}{\partial x}\left(\frac{Q^2}{H-b} + \frac{1}{2}gH^2 - gbH\right) = -gH\frac{\partial b}{\partial x} + \widetilde{S}(x,t). \end{cases} \tag{15}$$

Table 3
Convergence rates study for the steady and smooth case, Gaussian bed profile $b(x) = b_{\max} \cdot \exp[-\frac{(x-L/2)^2}{(L/2)^2}]$ and $b_{\max} = 0.001$ m, $Q = 1\ \mathrm{m^2\ s^{-1}}$, $H(x = L) = 1$ m, $L = 10$ m, CFL = 0.9

Method	N	$L_{1\,\mathrm{error}}$	$L_{1\,\mathrm{order}}$	$L_{\infty\,\mathrm{error}}$	$L_{\infty\,\mathrm{order}}$
ADER 2	5	0.357E−04		0.971E−04	
	10	0.117E−04	1.60	0.286E−04	1.76
	20	0.304E−05	1.94	0.818E−05	1.80
	40	0.760E−06	2.00	0.212E−05	1.94
	80	0.189E−06	2.00	0.542E−06	1.96
ADER 3	5	0.249E−04		0.759E−04	
	10	0.386E−05	2.69	0.852E−05	3.15
	20	0.550E−06	2.80	0.114E−05	2.89
	40	0.764E−07	2.84	0.171E−06	2.74
	80	0.104E−07	2.86	0.337E−07	2.34
ADER 4	5	0.160E−04		0.454E−04	
	10	0.196E−05	3.02	0.468E−05	3.27
	20	0.307E−06	2.67	0.190E−05	1.30
	40	0.447E−07	2.78	0.268E−06	2.82
	80	0.512E−08	3.12	0.487E−07	2.46
ADER 5	5	0.131E−04		0.375E−04	
	10	0.894E−06	3.87	0.208E−05	4.16
	20	0.423E−06	1.07	0.347E−05	−0.78
	40	0.550E−07	2.94	0.687E−06	2.33
	80	0.533E−08	3.36	0.108E−06	2.66

The exact expression of the source term $\widetilde{S}(x,t)$ is given by

$$\begin{aligned}\widetilde{S}(x,t) = {} & 4\pi \frac{a_0 \sin(\lambda x)\sin(\omega t)\left(Q_0 - \frac{a_0 L}{T_0}\sin(\omega t)\cos(\lambda x)\right)}{T_0(H_0 + a_0\cos(\omega t)\sin(\lambda x) - b_0\sin(\lambda x))} \\ & - \frac{2\pi\left(\frac{a_0}{L}\cos(\omega t)\cos(\lambda x) - \frac{b_0}{L}\cos(\lambda x)\right)\left(Q_0 - \frac{a_0 L}{T_0}\sin(\omega t)\cos(\lambda x)\right)^2}{(H_0 + a_0\cos(\omega t)\sin(\lambda x) - b_0\sin(\lambda x))^2} + 2\pi g\frac{a_0}{L}\cos(\omega t) \\ & \times \cos(\lambda x)(H_0 + a_0\cos(\omega t)\sin(\lambda x)) - 2\pi g\frac{a_0 b_0}{L}\cos(\omega t)\cos(\lambda x)\sin(\lambda x) - 2\pi\frac{a_0 L}{T_0^2}\cos(\omega t) \\ & \times \cos(\lambda x), \end{aligned} \tag{16}$$

where $\lambda = \frac{2\pi}{L}$ and $\omega = \frac{2\pi}{T_0}$.

As for the steady case we have performed numerical tests using sufficiently small values for the amplitudes a_0 and b_0, such that the non linearities appearing in the equations (in particular in the expression for the momentum flux) do not play a significant role. In Tables 4 and 5, we report the test case for $a_0 = 0.001$ m, $b_0 = 0.001$ m and $a_0 = 0.01$ m, $b_0 = 0.01$ m, respectively. The prescribed order of accuracy is reached for the schemes up to fourth order, as for the steady test case. Difficulties are observed for the fifth-order scheme even if it gives the smallest errors. This behaviour might be due to the non-linearities appearing in the equations; it does not seem to be related to the precision of the machine: tests using a quad-precision version of the code has been performed. We remark that we have also performed a convergence rates study, not reported here, for the model advection–reaction equation $\frac{\partial q}{\partial t} + \lambda\frac{\partial q}{\partial x} = \beta q$, with constant λ and β. The results for schemes of second to fifth order of accuracy are quite consistent with those for the non-linear inhomogeneous system.

6. Summary and concluding remarks

We have proposed a framework for constructing arbitrary high-order numerical schemes for the solution of the shallow water equations with source terms. A basic ingredient of the method is a high-order non-linear

Table 4
Convergence rates study for the unsteady and smooth case, $b_0 = 0.001$ m, $a_0 = 0.001$ m, $Q_0 = 1$ m^2 s^{-1}, $T_0 = 10$ s, CFL = 0.9

Method	N	L_1 error	L_1 order	L_∞ error	L_∞ order
ADER 2	5	0.152E−03		0.335E−03	
	10	0.391E−04	1.96	0.803E−04	2.06
	20	0.804E−05	2.28	0.180E−04	2.16
	40	0.182E−05	2.15	0.403E−05	2.16
	80	0.433E−06	2.07	0.951E−06	2.08
ADER 3	5	0.654E−04		0.126E−03	
	10	0.652E−05	3.33	0.150E−04	3.07
	20	0.103E−05	2.66	0.210E−05	2.83
	40	0.132E−06	2.96	0.269E−06	2.97
	80	0.163E−07	3.02	0.333E−07	3.01
ADER 4	5	0.381E−04		0.842E−04	
	10	0.267E−05	3.84	0.561E−05	3.91
	20	0.138E−06	4.27	0.306E−06	4.19
	40	0.718E−08	4.27	0.203E−07	3.91
	80	0.846E−09	3.09	0.207E−08	3.30
ADER 5	5	0.163E−04		0.377E−04	
	10	0.521E−06	4.97	0.118E−05	5.01
	20	0.159E−07	5.04	0.333E−07	5.16
	40	0.328E−08	2.28	0.463E−08	2.86
	80	0.909E−09	1.85	0.113E−08	2.03

reconstruction procedure based on the spatial cell averages. Here we have used the ENO method [13], instead of the more popular WENO method [20]. The ENO technique has an important advantage in that the high-order polynomial is known in the entire cell and its evaluation at all required integration points is straightforward. The WENO technique on the other hand has some disadvantages in the presence of source terms. The second ingredient of the ADER approach is the solution of the derivative Riemann problem including source terms, which as part of it, requires the use of the Cauchy–Kowalewski procedure, illustrated in the Appendix.

We have systematically assessed the methods presented. They satisfy the $\mathcal{Z}$-property, that is, they produce the exact stationary solution for an horizontal free surface elevation and vanishing velocities, as shown in Fig. 2. For the steady case the schemes have been shown, empirically, to converge to the correct solution and therefore, they satisfy the approximate $\mathcal{C}$-property. Steady solutions are well reproduced both in the smooth and in the discontinuous case, noting however, that in the case of steady discontinuous solutions, a refinement of the mesh does not always give better numerical results around discontinuities, except for the fortuitous case when the discontinuity is aligned with the interface between two adjacent cells.

An important aspect of this paper is the high accuracy in space and time for hyperbolic systems with source terms. Here we have implemented and tested schemes up to fifth order of accuracy in space and time and we have paid a great deal of attention to the practical verification of the theoretical expected orders of accuracy of the schemes. We have performed a study of the convergence rates of the schemes for tests with small amplitude sinusoidal distributions, both for the steady and for the unsteady cases. For situations in which the unknown functions exhibit large (of high order) derivatives we experienced some difficulties in achieving the expected convergence rates. We believe that non-linear terms in the governing equations are an additional contributing factor in explaining these difficulties. This combination of factors is likely to trigger and enhance the influence of round off errors. We speculate that another contributing factor could be due to the ENO interpolation procedure. In fact, closely associated schemes [5] based on WENO, rather than ENO, reconstructions have been shown to achieve the theoretically expected orders of accuracy.

We also note that results for the linear inhomogeneous model equations, not unreported here, are quite consistent with those of the non-linear inhomogeneous system case, in terms of the behaviour of even- and odd-order schemes and of the influence of large, high-order derivatives in the solution or in the bottom variation function. It is also worth remarking, however, that for the linear model case the notionally second-order scheme does not reach second order of accuracy, whereas for the non-linear system case the scheme achieves

Table 5
Convergence rates study for the unsteady and smooth case, $b_0 = 0.01$ m, $a_0 = 0.01$ m, $Q_0 = 1\ m^2\ s^{-1}$, $T_0 = 10$ s, CFL = 0.9

Method	N	$L_{1\,\text{error}}$	$L_{1\,\text{order}}$	$L_{\infty\,\text{error}}$	$L_{\infty\,\text{order}}$
ADER 2	5	0.152E−02		0.333E−02	
	10	0.389E−03	1.96	0.795E−03	2.06
	20	0.802E−04	2.27	0.180E−03	2.13
	40	0.181E−04	2.14	0.405E−04	2.15
	80	0.433E−05	2.06	0.946E−05	2.09
ADER 3	5	0.663E−03		0.125E−02	
	10	0.648E−04	3.35	0.149E−03	3.07
	20	0.102E−04	2.66	0.210E−04	2.82
	40	0.132E−05	2.95	0.271E−05	2.95
	80	0.164E−06	3.00	0.341E−06	2.98
ADER 4	5	0.372E−03		0.825E−03	
	10	0.277E−04	3.74	0.586E−04	3.81
	20	0.143E−05	4.27	0.311E−05	4.23
	40	0.841E−07	4.09	0.215E−06	3.85
	80	0.108E−07	2.95	0.223E−07	3.26
ADER 5	5	0.163E−03		0.374E−03	
	10	0.542E−05	4.91	0.125E−04	4.89
	20	0.203E−06	4.73	0.463E−06	4.76
	40	0.391E−07	2.37	0.630E−07	2.87
	80	0.103E−07	1.91	0.153E−07	2.03

second order of accuracy. For discontinuous solutions the numerical methods produce essentially non-oscillatory numerical results.

Finally, a remark regarding the justification of high-order methods, such as those of this paper, is due. Obviously, for a given mesh, a solution computed with a high-order method will give a smaller error, but the cost (measured in various ways) will be greater. So the crucial question is this: to attain a prescribed error deemed acceptable, is it more efficient to use a low-order method on a fine mesh or a high-order method on a coarse mesh? Recent studies of high-order ADER schemes show that higher-order schemes are more efficient, when computing solutions with high accuracy (small errors). For the linear case studied in [7] the authors report on a careful assessment of ADER schemes of up to 24th order of accuracy, as applied to acoustic problems in two space dimensions. The study shows that for computed solutions with a pre-assigned relatively large error, it is unclear as to whether it is more efficient to use a low-order method on a fine mesh or a high-order method on a coarse mesh. However, for computing a solutions with a small pre-assigned error it is distinctly more efficient to use high-order methods, and by a huge margin. Similar conclusions can be drawn for the non-linear case. In [5] the authors report on results for the three-dimensional non-linear Euler equations on unstructured meshes.

Acknowledgments

Part of this work was carried out while the third author was an **EPSRC senior visiting fellow** (Grant GR N09276) at the Isaac Newton Institute for Mathematical Sciences, University of Cambridge, UK, as joint organizer (with P.G. LeFloch and C.M. Dafermos) of the research programme *Non-linear Hyperbolic Waves in Phase Dynamics and Astrophysics*, Cambridge, January to July 2003. The support provided is gratefully acknowledged. The first and second authors acknowledge the support of the Italian Ministry of Higher Education and Research via the PRIN-2004 research project "Sviluppo di metodi numerici per applicazioni a problemi di fluidodinamica ambientale".

Appendix. Illustration of the Cauchy–Kowalewski procedure

System (2) can be rewritten in non-conservative form as follows:

$$\begin{cases} \frac{\partial H}{\partial t} + \frac{\partial Q}{\partial x} = 0, \\ \frac{\partial Q}{\partial t} + (gD - u^2)\frac{\partial H}{\partial x} + 2u\frac{\partial Q}{\partial x} = -u^2\frac{\partial b}{\partial x}, \end{cases} \tag{17}$$

which can be written in vectorial form as follows:

$$\partial_t \mathbf{U} + \mathbf{A}\partial_x \mathbf{U} = \overline{\mathbf{S}}, \tag{18}$$

where $\mathbf{A}$ is the matrix:

$$\mathbf{A} = \begin{bmatrix} 0 & 1 \\ gD - u^2 & 2u \end{bmatrix} \tag{19}$$

and the source term $\overline{\mathbf{S}}$ reads

$$\overline{\mathbf{S}} = \begin{bmatrix} 0 \\ -u^2\frac{\partial b}{\partial x} \end{bmatrix}. \tag{20}$$

To obtain the time derivatives for the evaluation of the numerical flux according to (8)–(11) it is necessary to write the time derivatives as functions of the spatial derivatives, using the Cauchy–Kowalewski procedure. As away we illustrate the method we give here the expressions for the time derivatives up to third order:

$$\begin{cases} \frac{\partial H}{\partial t} = -\frac{\partial Q}{\partial x}, \\ \frac{\partial Q}{\partial t} = -(gD - u^2)\frac{\partial H}{\partial x} - 2u\frac{\partial Q}{\partial x} - u^2\frac{\partial b}{\partial x}, \end{cases} \tag{21}$$

$$\begin{cases} \frac{\partial^2 H}{\partial t^2} = u^2\frac{\partial^2 b}{\partial x^2} + (gD - u^2)\frac{\partial^2 H}{\partial x^2} + 2u\frac{\partial^2 Q}{\partial x^2}, \\ \frac{\partial^2 Q}{\partial t^2} = (gD + 3u^2)\frac{\partial^2 Q}{\partial x^2} + 2u^3\frac{\partial^2 b}{\partial x^2} + 2u(gD - u^2)\frac{\partial^2 H}{\partial x^2}, \end{cases} \tag{22}$$

$$\begin{cases} \frac{\partial^3 H}{\partial t^3} = -2u^3\frac{\partial^3 b}{\partial x^3} - 2u(gD - u^2)\frac{\partial^3 H}{\partial x^3} - (gD + 3u^2)\frac{\partial^3 Q}{\partial x^3}, \\ \frac{\partial^3 Q}{\partial t^3} = -4u(gD + u^2)\frac{\partial^3 Q}{\partial x^3} - u^2(gD + 3u^2)\frac{\partial^3 b}{\partial x^3} - (gD + 3u^2)(gD - u^2)\frac{\partial^3 H}{\partial x^3}. \end{cases} \tag{23}$$

References

[1] A. Bermúdez, M.E. Vázquez-Cendón, Upwind methods for hyperbolic conservation laws with source terms, Comput. Fluids 23 (1994) 1049–1071.

[2] R. Bernetti, V.A. Titarev, E.F. Toro, Exact solution of the Riemann problem for the shallow water equations with discontinuous bottom geometry, Technical Report NI06020-NPA, Isaac Newton Institute for Mathematical Sciences, University of Cambridge, UK, 17 May, 2004. J. Comput. Phys., accepted for publication.

[3] N. Crnjaric-Zic, S. Vukovic, L. Sopta, Balanced finite volume WENO and central WENO schemes for the shallow water and the open-channel flow equations, J. Comput. Phys. 200 (2) (2004) 512–548.

[4] M. Dumbser, Arbitrary high order schemes for the solution of hyperbolic conservation laws in complex domains, PhD thesis, Institut für Aero-und Gasdynamik, Universität Stuttgart, Germany, 2005.

[5] M. Dumbser, M. Käser, V.A. Titarev, E.F. Toro, Quadrature-free non-oscillatory finite volume schemes on unstructured meshes for nonlinear hyperbolic systems, J. Comput. Phys. 226 (2007) 204–243.

[6] M. Dumbser, C.D. Munz, ADER discontinuous Galerkin schemes for aeroacoustics, C.R. Méc. 333 (2005) 683–687.

[7] M. Dumbser, T. Schwartzkopff, C.D. Munz, Arbitrary high order finite volume schemes for linear wave propagation, Notes on Numerical Fluid Mechanics and Multidisciplinary Design (NNFM), vol. 91, Springer, 2006, pp. 129–144.

[8] L. Fraccarollo, E.F. Toro, A shock-capturing method for two dimensional dam-break problems, in: Proceedings of the Fifth International Symposium in Computational Fluid Dynamics, Sendai, Japan, 1993.

[9] L. Fraccarollo, E.F. Toro, Experimental and numerical assessment of the shallow water model for two-dimensional dam-break type problems, J. Hydraul. Res. 33 (1995) 843–864.

[10] P. Garcia-Navarro, F. Alcrudo, 1D open channel flow simulation using TVD McCormack scheme, J. Hydraul. Eng., ASCE 118 (1992) 1359–1372.

[11] P. Garcia-Navarro, M.E. Vázquez-Cendón, On numerical treatment of the source terms in the shallow water equations, Comput. Fluids 29 (2000) 951–979.

[12] S.K. Godunov, Finite difference methods for the computation of discontinuous solutions of the equations of fluid dynamics, Mat. Sb. 47 (1959) 271–306.

[13] A. Harten, B. Engquist, S. Osher, S.R. Chakravarthy, Uniformly high order accuracy essentially non-oscillatory schemes III, J. Comput. Phys. 71 (1987) 231–303.

[14] M. Käser, Adaptive methods for the numerical simulation of transport processes, PhD thesis, Institute of Numerical Mathematics and Scientific Computing, University of Munich, Germany, 2003.
[15] M. Käser, A. Iske, ADER schemes for the solution of conservation laws on adaptive triangulations, Mathematical Methods and Modelling in Hydrocarbon Exploration and Production, Springer-Verlag, 2005, ISBN 978-3-540-22536-2.
[16] M. Käser, A. Iske, ADER schemes on adaptive triangular meshes for scalar conservation laws, J. Comput. Phys. 205 (2) (2005) 486–508.
[17] T. Schwartzkopff, Finite-Volumen Verfahren hoher Ordnung und heterogene Gebietszerlegung für die numerische Aeroakustik, PhD thesis, Institut für Aero-un Gasdynamik, Universität Stuttgart, Germany, 2005.
[18] T. Schwartzkopff, C.D. Munz, E.F. Toro, ADER: high-order approach for linear hyperbolic systems in 2D, J. Sci. Comput. 17 (2002) 231–240.
[19] T. Schwartzkopff, M. Dumbser, C.D. Munz, Fast high-order ADER schemes or linear hyperbolic equations, J. Comput. Phys. 197 (2004) 532–539.
[20] C.W. Shu, Essentially non-oscillatory and weighted non-oscillatory schemes for hyperbolic conservation laws, Technical Report ICASE Report No. 97-65, NASA, 1997.
[21] Y. Takakura, E.F. Toro, Arbitrarily accurate non-oscillatory schemes for a non-linear conservation law, J. Comput. Fluid Dyn. 11 (1) (2002) 7–18.
[22] V.A. Titarev, E.F. Toro, ADER: arbitrary high order Godunov approach, J. Sci. Comput. 17 (2002) 609–618.
[23] V.A. Titarev, E.F. Toro, ADER schemes for shallow water equations with pollutant transport, in: XXIX Convegno di Idraulica e Costruzioni Idrauliche, Trento, Italy, 7–10, September 2004, Editorial Bios, 2004, pp. 909–914.
[24] V.A. Titarev, E.F. Toro, ADER schemes for three-dimensional hyperbolic systems, J. Comput. Phys. 204 (2005) 715–736.
[25] E.F. Toro, Application of the weighted average flux method to the shallow water equations, in: B. Engquist, B. Gustafson (Eds.), Proceedings of the Third International Conference on Hyperbolic Problems, vol. 2, Chartwell-Bratt, 1991, pp. 874–887.
[26] E.F. Toro, Riemann problems and the WAF method for solving the two-dimensional shallow water equations, Philos. Trans. Roy. Soc. London, Ser. A 338 (1992) 43–68.
[27] E.F. Toro, Shock-Capturing Methods for Free-Surface Shallow Flows, Wiley and Sons Ltd., 2001.
[28] E.F. Toro, R.C. Millington, L.A.M. Nejad, Towards very high-order Godunov schemes, in: E.F. Toro (Ed.), Godunov Methods: Theory and Applications. Edited Review, Kluwer Academic/Plenum Publishers, 2001, pp. 905–937.
[29] E.F. Toro, V.A. Titarev, Solution of the generalised Riemann problem for advection–reaction equations, Proc. Roy. Soc. London, Ser. A 458 (2002) 271–281.
[30] E.F. Toro, V.A. Titarev, ADER schemes for scalar hyperbolic conservation laws with source terms in three space dimensions, J. Comput. Phys. 202 (1) (2005) 196–215.
[31] E.F. Toro, V.A. Titarev, Derivative Riemann solvers for systems of conservation laws and ADER methods, J. Comput. Phys. 212 (1) (2006) 150–165.
[32] M.E. Vázquez-Cendón, Improved treatment of source terms in upwind schemes for the shallow water equations in channels with irregular geometry, J. Comput. Phys. 148 (1999) 497–526.
[33] J.G. Zhou, D.M. Causon, C.G. Mingham, D.M. Ingram, The surface gradient method for the treatment of source terms in the shallow-water equations, J. Comput. Phys. 168 (2001) 1–25.
[34] C. Zoppou, S. Roberts, Explicit schemes for dam-break simulations, ASCE, J. Hydraul. Eng. 129 (1) (2003) 11–34.